Atmos. Meas. Tech. Discuss., 5, 5787–5822, 2012
www.atmos-meas-tech-discuss.net/5/5787/2012/
doi:10.5194/amtd-5-5787-2012

Atmospheric Measurement Techniques Discussions

Cirrus crystal fall velocity estimates using the Match method with ground-based lidars: a first case study

D. Dionisi[1,2], P. Kekchut[1], C. Hoareau[1], N. Montoux[3], and F. Congeduti[2]

[1]Laboratoire "Atmosphères, milieux, observations spatiales" (LATMOS), UMR8190, CNRS/INSU, UVSQ-UPMC, Guyancourt, France
[2]Institute of Atmospheric Science and Climate, Rome, Italy
[3]Laboratoire de Météorologie Physique, Blaise Pascal University, Aubiere, France

Received: 18 May 2012 – Accepted: 27 July 2012 – Published: 20 August 2012

Correspondence to: D. Dionisi (davide.dionisi@latmos.ipsl.fr)

Published by Copernicus Publications on behalf of the European Geosciences Union.

Abstract

Cirrus ice particle sedimentation velocity (v_r) is one of the critical variables for the parameterization of cirrus properties in a global climate model (GCM). In this study a methodology to estimate cirrus properties, such as crystal mean fall speed, through successive lidar measurements is evaluated. This "Match" technique has been applied on cirrus cloud observations and then tested with measurements from two ground-based lidars located in the Mediterranean Area. These systems have similar instrumental characteristics, and are operated manually respectively at the Observatory of Haute Provence (OHP, 43.9° N, 5.7° E) in France and at Rome Tor Vergata (RTV, 41.8° N, 12.6° E) in Italy at a distance of approximately 600 km providing systematic measurements since several years. The both sites are along a typical direction of an air path and a test case of an upper tropospheric cirrus, observed over both sites during the night between 13 and 14 of March 2008, has been identified and investigated. The analysis through lidar primarily parameters (cloud shape and vertical location) reveals a case of a thin sub-visible cirrus (SVC) located around the tropopause. The feasibility to estimate crystal fall velocity has been tested and values of 1.4–1.9 cm s^{-1}, consistent with simple-shaped small crystals, have been retrieved. Despite several uncertainties that affect the single-wavelength lidar measurements, sedimentation could be a partial reason for the cirrus property changes (e.g. geometrical thickness and back-scattering profile distribution) observed from one site to the other. The backward trajectory analysis suggests a type of cirrus formed by large-scale transport processes (adiabatic cooling of moist air masses coming from the subtropical area around Mexico gulf), which is characterized by a long atmospheric lifetime and horizontal extension of several hundreds of km.

This study shows that such approach can be improved in using closer locations, ancillary data (e.g. temperature, water vapour, etc.), particle distribution utilizing multi-wavelengths space-borne lidar measurements or balloon size particle and cirrus microphysical-resolved models.

AMTD
5, 5787–5822, 2012

1 Introduction

Sedimentation of ice crystal fall is an important process in clouds and has a large influence on their microphysical properties. In-situ measurements (Heymsfield and Miloshevich, 2003) have shown that the top of a cirrus cloud is mainly composed of small but numerous ice crystals, whereas the bottom more consists of few large crystals. Such vertical distributions can have some local cooling or warming radiative effects (Khvorostyanov and Sassen, 2002). In a study that relates climate sensitivity to atmospheric global climate model (GCM) parameters, Sanderson et al. (2008) identified the ice fall speed as the second most influential parameter to climate sensitivity and a decrease in fall speed was related to an increase in cirrus cloud coverage, humidity and long-wave cloud forcing. Similar conclusions were obtained using Lagrangian numerical simulations (Montoux et al., 2010). It has been also demonstrated (Jakob, 2002) that, in the weather forecast model of the European Centre for Medium Range Weather Forecast (ECMWF), the global mean integral radiation flux divergence decreases from $110\,\mathrm{W\,m^{-2}}$ to $90\,\mathrm{W\,m^{-2}}$ for assumed fixed values of the crystal fall speed from 0.1 to $2\,\mathrm{m\,s^{-1}}$. The importance of a correct representation of the sedimentation in large-scale models appears clearly when comparing the difference of $20\,\mathrm{W\,m^{-2}}$ with the $3.5\,\mathrm{W\,m^{-2}}$ radiative forcing due to the greenhouse effect for doubling CO_2. Sedimentation is also important in the evolution of the cloud structure and in the humidity field inside the cirrus as sedimenting ice crystals can quench in-cloud nucleation (Spichtinger and Gierens, 2009).

One of the main missing pieces of information for the determination of cirrus impacts was, up to recently, the altitude characterization of their vertical location and stratification. Cirrus clouds that consist of a small number of particles exhibit large scattering but tenuous optical depth. Space-borne passive remote sensing instruments in the infrared are nearly blind for a large part of these clouds due to their low sensitivity (Stubenrauch et al., 1999). On the contrary, active remote sensing methods based on lidar can detect high and thin cirrus clouds with high vertical spatial and temporal

AMTD
5, 5787–5822, 2012

resolution. Lidar measurements give access to cirrus backscattering vertical profile, from which it is possible to derive directly their absolute geometric height and thickness with typical resolutions of 10 to 100 m (Sassen and Wang, 2008). Backscattering ratio, which is related to the number of particles, their size, shape, composition and phase, can provide, with some assumptions, information about these quantities. Lidar can be operated continuously and then gives some indications of the variability of the cirrus above the instrument. For ground-based measurements, this variability is mainly related to advection and to the cirrus life cycle, as cirrus particles are both transported by the mean flow and subjected to ice crystals formation processes. Several statistics have been derived from these measurements (Goldfarb et al., 2001; Sassen et al., 2001; Cadet et al., 2005), but the global coverage of these observations, although they can provide useful information about the occurrence and cirrus types, is too poor to deduce accurate global radiative estimates. Similar measurements are now available from space with the Calipso mission (Sassen et al., 2009; Taylor et al., 2011) showing good agreement with ground-based stations (Dupont et al., 2010), providing a better knowledge of the horizontal distribution of the ice clouds (Chepfer et al., 2008). However, these measurements do not provide directly information about the life cycle of the cirrus clouds.

Ice particle growth, sedimentation, aggregation, light absorption, and evaporation could be investigated using a Lagrangian tracking method. The detailed locations and so the history of individual ice particle clusters and physical properties should be tracked as a function of time. This method, known as Match method (von der Gathen et al., 1995), consists in making a measurement at a given place and time, using forward trajectory to see if the sounded air mass will transit, by chance, over another sites equipped with similar instruments, and making a second measurement of the same air mass at the corresponding time matching with the forecast trajectory.

Observations from different locations within a given region of interest, coupled with Lagrangian trajectories, were developed to quantify chemical ozone loss in the Arctic stratosphere (Rex et al., 1998, 1999) using ozonesondes, then applied on water

AMTD
5, 5787–5822, 2012

vapour satellite data (Luo and Rossow, 2004), and, more recently, on Polar Stratospheric Clouds (PSC) studies during the International Polar Year (IPY).

The objective of this study has been to assess the feasibility of a possible future observing strategy that couples lidar measurements to a Lagrangian tracking method to study cirrus cloud formation and in particular here cirrus fall speed. The Eulerian characteristics of lidar technique, its typical temporal and vertical resolution in upper troposphere (tens of minutes and of meters) together with cirrus high horizontal variability do not allow deriving sedimentation velocity through measurements of only one lidar. In fact, to appreciate the sedimentation speed of cirrus crystals (between 0.01–10 $cm\,s^{-1}$) during a single lidar session with a vertical resolution of 75 m, lidar measurements should last, at least, two or three hours and, within this period, cirrus clouds should exhibit a negligible variability in order to explain changes in cirrus mean height only with crystal fall speed.

From space, passive measurements do not retrieve cloud altitudes accurate enough for such investigations. The proposed observing strategy could be to use several lidar systems and a trajectory tracking method in order to measure the same cirrus cloud at different time and then, because of advection, at different places. Exploiting the high resolution of lidar measurements to characterize cirrus vertical structures and the so-called Match technique, the idea is to apply this methodology to investigate the mean changes of the macrophysical cloud properties over quasi-stationary cloud periods (Hoareau et al., 2009) through the analysis of the variations of the derived lidar parameters observed by successive measurements located along the estimated directions of the air mass trajectory. In particular the vertical shape of the cirrus over few hours of transport, can be associated with crystal vertical distribution and, partly, to the sedimentation velocity.

The advanced lidar systems at Observatory of Haute-Provence (OHP) and at Rome-Tor Vergata (RTV), located respectively in the south of France and in Central Italy, are located at a reciprocal distance of 600 km, along a typical direction of front progression in the Mediterranean area. These geographical favourable conditions and the

AMTD
5, 5787–5822, 2012

instrumental similarity suggested testing Match-lidar cirrus technique in analysing the existing datasets of these two systems.

Thus, in this work, a subsample of the dataset of two lidars have been processed with a common algorithm procedure and coupled with a trajectory analysis. A test case of upper tropospheric thin cirrus measured over the two sites has been identified and analyzed with this Match strategy.

The paper is organized as follows: in Sect. 2 the main instrumental characteristics of the both lidar systems are briefly described together with the cirrus retrieval algorithms, while Sect. 3 addresses the Match-lidar methodology itself. The results of this approach are provided in Sect. 4, where the developed procedure is applied to the both lidar datasets. A test case of an upper tropospheric cirrus observed by the two systems during the night between 13 and 14 of March 2008 is studied. The associated uncertainties and the case consistency are discussed. Finally, in Sect. 5, the results, the limitations and the improvements required to adopt quantitatively this technique are discussed as a preparation of the setup of specific campaigns performed on alert.

2 Lidar systems description and retrieval of cirrus characteristics

At the OHP (43.9° N, 5.7° E, and 678 m altitude) a program of systematic lidar soundings of stratosphere and troposphere has been running for two decades (Goldfarb et al., 2001). The system utilizes a doubled Nd : YAG laser, which emits a light pulse of ∼10 ns at 532.2 nm, with 50 Hz repetition rate and 300 mJ average pulse energy. The receiver employs a multiple collecting telescope configuration for NDACC (Network for the Detection of Atmospheric Composition Changes) operations. For the Upper Troposphere Lower Stratosphere (UTLS) soundings, a single receiving telescope (20 cm diameter) with an adjustable diaphragm to reduce the collector efficiency is used. Transmitted beam and receiver field of view are zenith oriented. The photon counting system has a 0.5 ms bin width, corresponding to an altitude resolution of 75 m; the received backscatter signal is generally averaged over 160 s intervals. The

AMTD
5, 5787–5822, 2012

observations are performed at night. The lidar is operated for most of the weather permitting nights allowing cirrus detection between 100–150 nights per year. The typical time measurement period is 6 h. Raman channels for nitrogen and water vapour were also implemented (Sherlock et al., 1999). Atmospheric temperature measurements are taken from high-resolution (Vaisala RS92) radiosondes launched from Nimes, the closest meteorological station (∼ 80 km east of OHP).

The Rayleigh-Mie-Raman (RMR) lidar located in the suburban area of RTV (41.8° N, 12.6° E, and 107 m altitude), in the Institute of Atmospheric Sciences and Climate (ISAC), utilizes a Nd : YAG laser with second and third harmonic generators which emits two pulsed beams in the green (532.2 nm, 200 mJ energy per pulse) and in the UV (354.8 nm, 400 mJ energy per pulse), with 10 Hz repetition rate and ∼ 7 ns pulse width. The green beam is used to receive the elastic backscatter from the air molecules and aerosol particles; the UV beam is used to obtain Raman backscattering signals from water vapour and nitrogen molecules and to calculate the water vapour mixing ratio (Dionisi et al., 2010). Also in this case, a multiple telescope configuration is adopted in the receiver to collect the signal return from different altitude layers and obtain profiles of the interesting parameters over a wide altitude atmospheric interval (Congeduti et al., 1999). The acquisition vertical resolution is 75 m and the signals are integrated over 60 s (600 laser pulses) and recorded. The RMR system is operated in a manual mode and it provides 40–60 nighttime measurements per year. High-resolution radiosounding data (Vaisala RS92) are available from the Italian Meteorological Service in Pratica di Mare (25 km south-west of Tor Vergata). These are utilized for the calibration of the water vapour Raman profiles, and to add complementary parameters (e.g. density, temperature, etc.) to the lidar results. Technical characteristics of the two instruments are provided in Table 1.

In case of Match events (see Sect. 3), the same data analysis procedure is applied to the raw lidar data of the two instruments in order to detect the presence of cirrus and provide its vertical shape. In particular, this procedure consists in deriving the backscattering ratio (BSR, the ratio between the sum of the Mie and Rayleigh backscattering

AMTD
5, 5787–5822, 2012

coefficients and the Rayleigh backscattering coefficient) vertical profiles from the ratio between the return signal at 532 nm and nitrogen Raman signal (Ferrare et al., 2001) and in using this quantity to obtain the optical depth of the mid and upper atmosphere (between 7 and 12/13 km, approximately), assuming a fixed value of the lidar ratio (i.e. extinction-to-backscatter ratio, LR, Platt et al., 1984), with a temporal resolution of the original raw data.

In order to get a reasonable compromise between measurement accuracy and atmospheric variability, the time series of the optical depth are analysed through an iterative method designed to research discontinuity points in order to define periods of quasi-stationary conditions regarding statistical variability (Lanzante, 1996). Data analyses are then performed on these integrated periods to derive accurate optical cirrus properties (Hoareau et al., 2009). The backscattering profile retrieval is based on the methodology described in Goldfarb et al. (2001) for OHP lidar and slightly modified for the RMR Italian lidar, permitting to characterize cirrus clouds through some lidar principal parameters (LPP) such as the absolute geometric height, thickness, the mean backscattering ratio, the relative height to tropopause and the optical depth.

3 Description of the Match cirrus technique

As previously mentioned, the Match method was initially applied to estimate the chemical ozone loss on the Artic stratosphere and, more recently, to study PSC during IPY. The basic idea of a Match method is: after an air parcel has been probed at a given place and time (departure site), its forward trajectory is calculated; if the air mass transits over (or close to) another site (arrival site) that perform a second sampling with a similar instrument, then the two measurements form a “Match” and can be compared. The comparison of these two successive measurements of the same air mass gives direct information about its composition. A similar approach has been applied here to study cirrus evolution with two ground-based lidar stations, OHP and RTV, which are the departure and the arrival site, respectively. Associated with these lidar

AMTD
5, 5787–5822, 2012

measurements, two clusters of five trajectories (backward and forward) are launched for each site at three different altitudes (8, 10 and 12 km, respectively) corresponding to the 3 main cirrus cloud clusters (Keckhut et al., 2006) to find potential Match cases between the both sites in the upper troposphere. The central trajectory of each altitude starts at the lidar station and the other four trajectories are started 0.5° each to the north, south, east and west (approximately 55 km in latitude and 40 km in longitude), of the central one. Trajectories are considered reliable (not divergent) only if, at the ending point (i.e. at the arrival lidar station), the sum of the distances between the central and the other four trajectories does not exceed the initial sum of the distances at the starting lidar station of no more than 20 %.

Match cases are those fulfilling two fixed criteria:

- The nearest points to the arrival lidar station of the central trajectory for each of two clusters should be at a distance lower than a maximum value (R_{max}, spatial Match condition).
- The time spent by the air mass to move from one site to the other should be included within Δt_m which is the time lag defined by the lidar measurement starting time of the departure site and the lidar measurement ending time of the arrival site (temporal Match condition).

Uncertainties associated to the Match method are, in general, composed of systematic and random errors. Systematic errors are inherent in the measurement techniques adopted in Match method (in our case, lidar technique and the trajectory code). Referring to the four sources of random errors attached to the Match method used for ozone loss quantifications, identified by Lehmann et al. (2005), the successive campaigns were helpful, to improve the methodology based on the effort of identifying and reducing all the identified sources of error. Similar uncertainties exist when applying Match method to cirrus. Lidar technique itself with one wavelength does not introduce the largest uncertainty while the direct variables are used (altitude and optical depth) and depend on vertical resolution (here 75 m). Cluster trajectory approach even if used

AMTD
5, 5787–5822, 2012

in many applications, represent the largest uncertainties and rely on the accuracy of the meteorological analyses and mainly the vertical wind. The remaining two other error sources, non-zero match radius (i.e. spatial coincidence between the second lidar measurement and the calculated position of the air mass) and deviation between single measurements and mean quantities (i.e. representativeness of individual lidar sessions to describe cirrus mean variations), are two critical points because of the high temporal and spatial variability of cirrus. The contribution of the latter source can be reduced by the quasi-stationary integration approach described previously, which somehow give an average quantity of the location of the cloud that smooth the local variability due to inhomogeneities of temperature and water vapour fields (Keckhut et al., 2012). A suitable maximum match radius (R_{max}), instead, must be applied to limit the error contribution of the former source. However, the value of R_{max} strictly depends on the horizontal extension and variability of the cirrus; for the case considered in this work, R_{max} is fixed to 150 km.

If air masses fulfil these conditions and the presence of cirrus is revealed in both lidar datasets, the significant changes of cirrus mean optical characteristics can then be attributed to real changes of the cirrus vertical structures.

4 Results

4.1 French-Italian experimental setup

The French and the Italian lidar sites are located along one of the typical direction of the front progression in the Mediterranean area. This statement has been confirmed studying the origin of the air masses arriving daily above the RTV site at 00:00 UTC. In fact, using the GDAS (Global Data Assimilation System) dataset for five years (2006–2010), the 24-h backward trajectories for three different heights (8, 10 and 12 km, respectively) have been calculated through the Hybrid Single-Particle Lagrangian Integrated Trajectory (HYSPLIT, Draxler and Rolph, 2003) model, in order to determine the frequency of

AMTD
5, 5787–5822, 2012

occurrence of the air masses that passed over a 0.7° × 0.7° grid centred at OHP before arriving at RTV. This analysis has highlighted that the OHP–RTV direction (NO–SE) is one of the more frequent direction for the upper tropospheric air mass displacement in the Northwest Mediterranean region and more than 10 % of the air masses, which arrive at RTV at 00:00 UTC, have previously passed over OHP (OHP–RTV air mass coincidence).

The Fig. 1 depicts the cumulative occurrence (in %) of the time spent by the air masses (at 8,10 and 12 km, solid, dashed and dotted lines, respectively) to go from OHP to RTV, for the 2006–2010 period. It has to be noted that, for approximately 40 % of the cases (i.e. 4 % of the total number of backward trajectory considered), the time needed to cover the distance between the two sites (approximately 600 km) is lower or equal to 8 h. This value has been fixed as Δt_m. Therefore, during contemporary night-time lidar session, it is possible that the same upper tropospheric air mass has the time to advect from one site to the other one, thus fulfilling the temporal Match condition.

These geographical favourable conditions and the instrumental characteristics of OHP and RTV lidars (similar in terms of emitted wavelengths and capabilities) suggested testing Match-lidar cirrus strategy analysing the existing dataset of these two systems.

The first requirement consists to find cirrus cases extending or travelling from OHP to RTV in the dataset of both instruments. For this study, night-time lidar sessions of two-year period 2007–2008 have been considered. The statistics of the number of measurements observed by each lidar and the number of contemporary night-time measurements are resumed in Table 2.

Despite the OHP–RTV upper tropospheric favourite direction, the number of contemporary lidar measurements (and consequently the number of MATCH sessions) is significantly reduced by the manual-operating mode of the RMR measurement operations. In fact, out of 42 common day lidar sessions, only four cases, in which the upper tropospheric air masses successively passed over OHP and RTV sites, fulfilled the above-stated MATCH criteria and, in particular, since no coordinated operation was

AMTD
5, 5787–5822, 2012

performed at that time, only one case over both sites observed the presence of the same air mass including cirrus clouds. This case refers to the night between 13 and 14 March 2008 where an upper tropospheric thin cirrus has been measured by OHP and RTV lidars.

4.2 Test case description

Figure 2a and b reports the temporal evolution of the BSR measured for this night at OHP and RTV stations, respectively. White vertical lines indicate the quasi-stationary periods identified. According to the procedure described in Sect. 2, the combined use of the elastic and nitrogen Raman channel of the two systems allowed to characterize the cirrus observed through lidar principal parameters.

Table 3a and b gives the results of this analysis for each quasi-stationary period of the lidar sessions of the two sites. In particular, optical depth τ has been estimated independently using both the BSR profile inside the cirrus with a fixed a-priori value of LR (particle integration, PI, method, Cadet et al., 2006) and the comparison of the elastic backscattering signals, fitted through the radiosonde density profile, just below and above the cloud (molecular integration, MI, method, Chen et al., 2002). For the cirrus observed through the RTV lidar system, the amount of signal in the nitrogen channel permitted to evaluate τ using the extinction of Raman signal below and above the cirrus (Raman method, Ansmann et al., 1992). However, because of the very low optical thickness of the cirrus studied, the optical depths, calculated with MI and the Raman methods, are affected by large errors, as reported by Table 3a and b. The errors associated to optical depths are calculated following the appendix in Chen et al. (2002). Furthermore, it is worth noting that, in case of optically thin cirrus ($\tau \ll 1$, in the visible), the multiple scattering factor have an influence of less than 1 % in the estimation of τ, therefore no corrections of multiple scattering have been made. The temperature values inside the cirrus for OHP and RTV, as well as the density profiles, are derived from the operational radiosonde launched respectively from Nimes (80 km west from the OHP) and Pratica di Mare (25 km south-west from RTV). During the OHP lidar

AMTD
5, 5787–5822, 2012

session there is no presence of cirrus between 19:20 and 21:38 UTC, while cirrus is constantly present over RTV site with a case of two-layer cirrus for the first two hours.

The cirrus sensed through the OHP lidar has similar characteristics of those identified through RMR system. In particular both cirrus exhibit similar values of optical depth, mean altitude, thickness and intensity of the mean backscattering ratio. These values highlight the presence, over both sites, of a subvisible cirrus (SVC), which has an optical depth always below 0.03 (except for period 2 of the OHP), a thickness varying from 500 m and 1.3 km, an altitude between 10.8 and 11.4 km and a top height that is around the local tropopause (11.24 and 11.10 km for OHP and RTV, calculated using radiosonde temperature data and the definition of thermal tropopause).

The 3-D backward trajectories, corresponding to the height of the cirrus envelopes (from 10.7 km to 11.7 km), for the air-masses which pass above the OHP site at 19:00 UTC of 13 March 2008 and arrive near RTV site at 01:00 UTC of 14 March 2008 are shown in Fig. 3. For reason of clarity, for each altitude, only central backward trajectories of the reliable clusters are reported. The case considered satisfies both spatial (the air masses pass near the RTV site at about 80 km, within R_{max}) and temporal (the air mass advection time from one site to the other, 6 h approximately, is within Δt_m) Match conditions (see Sect. 2).

4.3 Test case characterization and discussions

The temporal evolution of height, temperature and potential temperature (z, T and θ, respectively) between 11 March 2008 at 01:00 UTC and 14 March 2008 at 01:00 UTC for the cirrus envelopes, considered in Fig. 3, are shown in Fig. 4. This figure reveals an essentially constant trend for θ during the whole evolution (air masses advect, roughly, along the same isentropic levels) excepting the slight fluctuation of $\approx 3/4$ K between the 15:00 UTC and 22:00 UTC of 13 March 2008 which can be due to noise in Hysplit model field and will be neglected. A coincident negligible fluctuation is observed in the last part of z and T air mass evolution. On the contrary, a relevant constant increase (decrease) between 11 March 2008 at 04:00 UTC and 12 March 2008 at 04:00 UTC

AMTD
5, 5787–5822, 2012

noticed when considering the z (T) evolution of cirrus envelopes, will be discussed afterwards.

The previous analysis allows assuming a quasi-isentropic air-mass transport between the two sites (between 13 March 2008 at 19:00 UTC and 14 March 2008 at 01:00 UTC, black horizontal bars in Fig. 4). This assumption together with the fulfilment of Match conditions permits to use the difference between the two cirrus heights (Δz_{cir}), measured by OHP and RTV lidars, corrected with the local isentropic shift ($\Delta z_{\mathrm{theta}}$), to estimate the cirrus mean sedimentation velocity (v_{s}) between the two sites, following the simplified equation:

$$v_{\mathrm{s}} = \left(\Delta z_{\mathrm{cir}} + \Delta z_{\mathrm{theta}}\right) / \Delta t, \tag{1}$$

where Δt is the time spent by the air mass to go from one site to the other. Thus, the first and the last quasi-stationary periods, respectively at the OHP and RTV (see Table 3a and b), whose temporal distance corresponds to Δt (approximately 6 h), have been compared. The backscattering ratio profiles of the two cirrus are reported in Fig. 5. The considered mid-cirrus height (z_{cir}) are defined as (Chen at al., 2002):

$$z_{\mathrm{cir}} = \frac{\int_{z_{\mathrm{base}}}^{z_{\mathrm{top}}} z' R(z') \mathrm{d}z'}{\int_{z_{\mathrm{base}}}^{z_{\mathrm{top}}} R(z') \mathrm{d}z'}, \tag{2}$$

namely the BSR mass centre of the cirrus (11.42 and 11.20 km, respectively for OHP and RTV periods, with $dz_{\mathrm{cir}} = 0.05$ km). Considering the height and isentropic shift (0.2 and approximately 0.1 km, respectively) between the two sites, v_{s} is approximately 1.5 cm s^{-1}.

Assuming that the terms of the sum in the right part of Eq. (1) are uncorrelated and if the uncertainty in Δt is neglected, the uncertainty (dv_{s}) is mainly due to the separation contribution of the errors of these terms. In this study it has been considered

AMTD
5, 5787–5822, 2012

only the uncertainty ($d\Delta z_{cir}$) associated to Δz_{cir}, so that $dv_s \approx d\Delta z_{cir}$, derived by the propagation error formula, is approximately 0.3 cm s^{-1}. Furthermore v_s is also affected by the fact that larger crystals, during the advection between the two sites, could have disappeared and reformed before the cirrus is above the arrival site, with the result that the value of v_s could be underestimated. In the case considered, in fact, the height of z_{cir} for OHP cirrus was calculated including a part of the cirrus (the large peak at 11.4 km in Fig. 5) that is likely to be composed by large crystals. To roughly estimate this systematic error, it has been assumed that only survival small crystals, which are mostly present in the upper part of the OHP cirrus, cause the cirrus vertical displacement observed between OHP and RTV. With this assumption z_{cir} at the OHP is equal to 11.51 km and the corresponding v_s is 1.9 cm s^{-1}.

Although, with single-wavelength measurements, it is not possible to distinguish which properties have been evolved between two successive measurements, changes of the backscatter signal and in optical depth could be most probably associated with change of the crystal size parameter during the advection (Jumelet et al., 2008). In particular, from the lidar values of the quasi-stationary periods considered in Table 3a and b and the Fig. 5, the cirrus, in addition to lower in altitude, appears to extend its vertical thickness (Δz from 0.5 to 0.7 km) and simultaneously decrease its optical depth (τ from 0.026 to 0.011, considering the values estimated with PI method) and the intensity of the mean BSC inside the cirrus (from 7.6 to 2.4). A similar variation in τ is not highlighted when comparing the values derived from the MI and Raman method, but the great uncertainty affecting these values did not allow making any further analysis. Using the values of Δz and τ measured by the two lidar stations, it is possible to roughly evaluate the crystal mean radius variation. In fact, assuming a uniform mono-dispersed size distribution throughout the cloud depth and a constant extinction efficiency (Q_e) of 2, the experimental ice crystal effective radius (r_{exp}) for various number concentrations (N_0) can be estimated, according to the following formula (Comstock et al., 2002):

AMTD
5, 5787–5822, 2012

$$r_{\mathrm{exp}} = \sqrt{\frac{\tau}{N_0 \cdot \Delta z \cdot Q_{\mathrm{e}} \cdot \pi}}, \tag{3}$$

The comparison between the values of r_{exp}, for the two considered periods, highlights, for ice crystal population with the same number concentration, an effective radius reduction of more than 50 % which might be caused by the ice crystal sedimentation into sub-saturated air below the cirrus. In fact, on average, this process decreases more the population of large ice crystals (which fall out of the cloud layer and sublimate), favouring the persistence of small ice crystals.

Utilizing the range of values 1.4–1.9 cm s^{-1} for v_{s} and following the Stokes equation, it is possible, assuming spherical shape, to calculate the theoretical mean radius (r_{th}) of crystals for the cirrus at the French departure site:

$$r_{\mathrm{th}} = \sqrt{\left(\frac{9}{2} \cdot \frac{v_{\mathrm{s}}\mu}{(\rho_{\mathrm{i}} - \rho_{\mathrm{a}})\, g}\right)}, \tag{4}$$

where μ is the dynamic viscosity of the air, ρ_{i} and ρ_{a} are respectively the mass density of ice and air and g is the gravitational acceleration. For the values of temperature and pressure, derived from Nimes radiosounding, r_{th} is equal to 9.9–11.5 µm. From the comparison of these values to the set of r_{exp} of Table 4 it is possible to deduce the corresponding values of N_0 and then to estimate qualitatively the OHP cirrus Ice Water Content (IWC), which is roughly 0.1–0.01 mg m^{-3}.

Analysing the relative position of BSR mass centre compared to the mean geometric height for the two periods considered can be useful to have rough information about the ice distribution. In particular, a possible explanation of the difference between the values found for OHP and RTV (0.46 and 0.55, respectively, where 0 represents the cirrus base and 1 the cirrus top position) could be that, because of the sedimentation and disappearance of larger crystals during the advection, the ice mass distribution,

AMTD
5, 5787–5822, 2012

which at OHP is centred around the peak in the lower part of the cirrus, at RTV is dominated by the presence of small crystals in the upper part of the cloud. However these values cannot be directly related to the size or to the number concentration of ice crystals and the measurements of other parameters (e.g. multi-wavelength backscattering and depolarization profiles) are required to quantitatively study the distribution of ice particle within the cirrus.

The value of v_s (1.4–1.9 cm s^{-1}), estimated for the cirrus observed by OHP and RTV lidar systems during the night from 13 to 14 March 2008, is consistent with the types of crystals that are likely to compose high altitude, optically thin, cold cirrus, namely crystals with simple shapes and small dimensions. Furthermore the qualitative values of r and IWC derived for the cirrus ($\approx$ 10 µm and 0.1–0.01 mg m^{-3}, respectively) studied are comparable to those observed for SVCs in other studies (Immler et al., 2008, for northern mid-latitude SVC and Davis et al., 2010, for a tropical tropopause SVC).

Following mid-latitude cirrus classification derived from the lidar data of the French site (Keckhut et al., 2006), the case considered belongs to the thin tropopause class, which is characterized by low values of temperature, thickness and optical depth and a location in correspondence of the local tropopause. Several case studies (Keckhut et al., 2005; Montoux et al., 2009) relate the formation of this class to large-scale transport processes (advection to mid-latitudes of clouds related to cumulonimbus clouds anvils or of moist tropical upper tropospheric air masses). This latter hypothesis (in particular the transport of moist air masses) could be the explanation for the formation of the considered cirrus. In fact the drop in temperature by approximately 10 K experienced by the air mass during their transit over the western and central part of Atlantic (see Fig. 4) corresponds to a slight air uplift of 1000 m in approximately 24 h (1.2 cm s^{-1}). This feature could be associated to an adiabatic process over Atlantic Ocean bringing wet air to upper regions of the troposphere. The adiabatic cooling, associated with the observed air mass upward motion, could have resulted in an increase of ice saturation and favoured the formation and the growth of ice crystal (Jensen et al., 1996; Boehm et al., 1999). Therefore the considered cirrus seems to relate to the air

AMTD
5, 5787–5822, 2012

transport of small scale filamentary structures extending for a couple of hundred of kilometers horizontally and with a vertical thickness of few kilometers (Keckhut et al., 2005). Furthermore, with the relatively small size of ice crystals (radii $\leq 5\,\mu m$) as in the case considered, cloud radiative heating could generate a circulation (with rising inside the cloud, sinking outside the cloud, entrainment at cloud base, detrainment at cloud top) which can provide a water supply for the cloud and substantially extend the cloud lifetime, as showed by Dinh et al. (2010).

From these considerations, it is clear that the developed cirrus observing strategy, in addition to the fulfilment of the Match conditions, is exploitable only to cirrus that have a large horizontal extension (hundred of km), long cloud lifetime (tens of hours) and a relatively small horizontal variability. However, these conditions are necessary but not sufficient to reliably assume the cirrus maintenance during the advection between the sites, in particular if the sites are relatively distant. In other words, to verify the processes to which cirrus crystals are subjected during the transport from one site to the other, further measurements are required. A possible tool to track cirrus advection could be the use of satellite data from passive space-borne instruments and/or from CALIOP (Cloud-Aerosol Lidar with Orthogonal Polarization), the space borne lidar installed on CALIPSO (Cloud Aerosol Lidar and Infrared Pathfinder Satellite Observation). In our case, the small optical thickness of the cirrus limited the use of passive sensors while coincident CALIOP lidar-tracks were not available. The employment of cirrus microphysical-resolved models (as Weather Research and Forecasting, WRF, Gu et al., 2011) should be also foreseen to simulate and monitor the evolution of cirrus properties between the two sites.

5 Conclusions

In this work, an observing strategy to study the evolution of cirrus optical properties has been investigated. This methodology, which couples lidar measurements through the Match approach, foresees to characterize mean significant changes in optical

AMTD
5, 5787–5822, 2012

properties of cirrus quasi-stationary periods from the analysis of the lidar parameter variations observed between successive measurements located along the direction of the air mass advection. To assess its feasibility, the technique has been tested on an existing subsample of dataset (2007–2008) of OHP and RTV lidars, which are located along one of the typical direction of the front progression in the Mediterranean area, and exhibiting similar instrumental characteristics, in terms of emitted wavelengths, data resolution and performances. Applying on this dataset a common algorithm procedure and the proposed cirrus Match approach, a test case of upper tropospheric thin cirrus observed by the two instruments during the night from 13 to 14 March 2008 has been identified and characterized. In particular, the assumption of a quasi-isentropic air-mass transport between the two sites together with the fulfilment of Match conditions allowed using the first and the last quasi-stationary periods, measured respectively above the OHP and RTV, to estimate the crystal cloud mean sedimentation velocity (v_s) between the two sites. The range of retrieved values for v_s (1.4–1.9 cm s^{-1}) is consistent with crystals of simple shapes and small dimensions. The uncertainty associated with this value, considering only the error of the term representing the difference between the two cirrus heights, is around 20 %. One of the critical point in this estimation, attested by a range bar of more than 30 %, is that, during advection, larger crystals, because of ice sedimentation, could have disappeared before the cirrus is above the arrival site, causing an underestimation of v_s. This effect has to be considered when calculating the cirrus height at the departing site.

Although several uncertainties affect the single-wavelength lidar measurements, this effect of the ice sedimentation, which favours more the persistence of small ice crystals than large ones, could partly explain the differences between the cirrus lidar principal parameters measured by the two stations in terms of cirrus vertical and optical thickness and the BSR profile distribution within the cirrus.

During the transport from one site to the other, cirrus crystals are subjected to modify their optical and physical properties. One of main uncertainty of the proposed method consists on the assumption of the cirrus maintenance during the advection between

AMTD
5, 5787–5822, 2012

the two sites. For the test-case considered, the backward trajectory analysis suggest a type of cirrus formed by large-scale transport processes (adiabatic cooling of moist air masses coming from the Atlantic Ocean), which is, usually, characterized by atmospheric lifetime of tens of hours and horizontal extension of several hundreds of km. These cirrus characteristics could partly justify this assumption, however a further condition on cirrus persistence between the measuring sites has to be added besides the adopted conditions on temporal and spatial coincidence of the lidar measurements.

In conclusion the developed Match-lidar method seems to be a valid tool to study the mean evolution of cirrus that have a large horizontal extension (hundred of km), long cloud lifetime (tens of hours) and a relatively small horizontal variability. The high vertical spatial and temporal resolution of lidar measurements together with a Lagrangian approach assure a characterization of cirrus optical parameters, in particular for those cirrus, as SVCs, that are hardly observable through space-borne passive instruments. However some improved requirements have to be adopted to reduce the uncertainties that affect the technique:

- lidar stations must be located along frequent directions of air mass displacements, at a maximum distance of 200–300 km that allows distinguishing changes in main cirrus optical properties and that, at the same time, assures an high probability of Match events and a cirrus persistence between the two sites;
- high temporal and spatial variability of cirrus is a critical issue of adopting Lidar-Match coupling to cirrus. To reduce the uncertainties associated to this variability, mean lidar quantities through the identification of quasi-stationary temporal periods have to be employed and a suitable match-radius (R_{max}), which depends on cirrus type, should be fixed;
- multi-wavelength lidar measurements are required to quantitatively characterize the differences of LPPs (e.g. geometrical and optical thickness, back-scattering profile distribution) observed between two sites;

AMTD
5, 5787–5822, 2012

– lidar data have to be integrated with ancillary measurements (in-situ and space-borne) of cirrus crystal size distribution, water vapour and temperature to characterize the processes to which cirrus are subjected during the transport from one site to another;

– in addition to spatial and temporal Match conditions, a further requirement on cirrus persistence has to be adopted. The fulfilment of this condition could be verified by the employment of CALIOP data to track cirrus advection, and by using a microphysical cirrus model (WRF) to monitor cirrus evolution between the two sites.

Acknowledgements. The authors thank Gian Luigi Liberti for the helpful discusssions and Federico Angelini for his support on backward trajectory statistical processing. The authors acknowledge the NOAA Air Resources Laboratory (ARL) for the provision of the HYPLIT transport and dispersion model. OHP lidar activities are supported both by INSU and CNES. The research leading to these results has received funding from the European Union Seventh Framework Programme (FP7/2007-2013) under grant agreement RBUCE-UP No. 246556.

The publication of this article is financed by CNRS-INSU.

AMTD
5, 5787–5822, 2012

References

Ansmann, A., Wandinger, U., Riebesell, M., Weitkamp, C., and Michaelis, W.: Independent measurement of extinction and backscatter profiles in cirrus clouds by using a combined Raman elastic-backscatter lidar, Appl. Optics, 31, 7113–7131, 1992.

Boehm, M. T., Verlinde, J., and Ackerman, T. P.: On the maintenance of high tropical cirrus, J. Geophys. Res., 104, 24423–24434, 1999.

Cadet, B., Giraud, V., Haeffelin, M., Keckhut, P., Rechou, A., and Baldy, S.: Improved retrievals of the optical properties of cirrus clouds by a combination of lidar methods, Appl. Optics, 44, 1726–1734, 2005.

Chen, W. N., Chiang, C. W., and Nee, J. W.: Lidar ratio and depolarization ratio for cirrus clouds, Appl. Optics, 41, 6470–6476, 2002.

Chepfer, H., Bony, S., Winker, D. M., Chiriaco, M., Dufresne, J.-L., and Seze, G.: Use of CALIPSO lidar observations to evaluate the cloudiness simulated by a climate model, Geophys. Res. Lett., 35, L15704, doi:10.1029/2008GL034207, 2008.

Comstock, J. M., Ackerman, T. P., and Mace, G. G.: Ground-based lidar and radar remote sensing of tropical cirrus clouds at Nauru Island: cloud statistics and radiative impacts, J. Geophys. Res., 107, 4714, doi:10.1029/2002JD002203, 2002.

Congeduti, F., Marenco, F., Baldetti, P., and Vincenti, E.: The multiple-mirror lidar "9-eyes", J. Opt. A-Pure Appl. Op., 1, 185–191, 1999.

Davis, S., Hlavka, D., Jensen, E., Rosenlof, K., Yang, Q., Schmidt, S., Borrmann, S., Frey, W., Lawson, P., Voemel, H., and Bui, T. P.: In situ and lidar observations of tropopause subvisible cirrus clouds during TC4, J. Geophys. Res., 115, D00J17, doi:10.1029/2009JD013093, 2010.

Dinh, T. P., Durran, D. R., and Ackerman, T.: The maintenance of tropical tropopause layer cirrus, J. Geophys. Res., 115, D02104, doi:10.1029/2009JD012735, 2010.

Dionisi, D., Congeduti, F., Liberti, G. L., and Cardillo, F.: Calibration of a multichannel water vapor raman lidar through noncollocated operational soundings: optimization and characterization of accuracy and variability, J. Atmos. Ocean. Tech., 27, 108–121, 2010.

Draxler, R. R. and Rolph, G. D.: HYSPLIT (Hybrid Single-Particle Lagrangian Integrated Trajectory) Model. NOAA ARL READY, NOAA Air Resources Laboratory, Silver Spring, MD, available at: http://ready.arl.noaa.gov/HYSPLIT.php (last access: 20 July 2012), 2003.

AMTD
5, 5787–5822, 2012

Dupont, J.-C., Haeffelin, M., Morille, Y., Noël, V., Keckhut, P., Winker, D., Comstock, J., Chervet, P., and Roblin, A.: Macrophysical and optical properties of midlatitude cirrus clouds from four ground-based lidars and collocated CALIOP observations, J. Geophys. Res., 115, D00H24, doi:10.1029/2009JD011943, 2010.

Ferrare, R. A., Turner, D. D., Heilman Brasseur, L., Feltz, W. F., Dubovick, O., and Tooman, T. P.: Raman lidar measurements of the aerosol extinction-to-backscatter ratio over the Southern Great Plains, J. Geophys. Res., 106, 20333–20347, 2001.

Goldfarb, L., Keckhut, P., Chanin, M.-L., and Hauchecorne, A.: Cirrus climatological results from lidar measurements at OHP, Geophys. Res. Lett., 28, 1687–1690, 2001.

Gu, Y., Liou, K. N., Ou, S. C., and Fovell, R.: Cirrus clouds simulations using WRF with improved radiation parameterization and increased vertical resolution, J. Geophys. Res., 116, D06119, doi:10.1029/2010JD014574, 2011.

Heymsfield, A. and Miloshevich, L.: Parameterizations for the cross-sectional area and extinction of cirrus and stratiform ice cloud particles, J. Atmos. Sci., 60, 936–956, 2003.

Hoareau, C., Keckhut, P., Sarkissian, A., Baray, J. L., and Durry, G.: Methodology for water monitoring in the upper troposphere with Raman lidar at Haute-Provence Observatory, J. Atmos. Ocean. Tech., 26, 2149–2160, 2009.

Immler, F., Treffeisen, R., Engelbart, D., Krüger, K., and Schrems, O.: Cirrus, contrails, and ice supersaturated regions in high pressure systems at northern mid latitudes, Atmos. Chem. Phys., 8, 1689–1699, doi:10.5194/acp-8-1689-2008, 2008.

Jakob, C.: Ice clouds in numerical weather prediction models, in: Cirrus, edited by: Lynch, D. K., Sassen, K., Starr, D. O'C., and Stephens, G., Oxford University Press, 327–345, 2002.

Jensen, E., Toon, O., Selkirk, H., Spinhirne, J., and Schoeberl, M.: On the formation and persistence of subvisible cirrus clouds near the tropical tropopause, J. Geophys. Res., 101, 21361–21375, 1996.

Jumelet, J., Bekki, S., David, C., and Keckhut, P.: Statistical estimation of stratospheric particle size distribution by combining optical modelling and lidar scattering measurements, Atmos. Chem. Phys., 8, 5435–5448, doi:10.5194/acp-8-5435-2008, 2008.

Keckhut, P., Hauchecorne, A., Bekki, S., Colette, A., David, C., and Jumelet, J.: Indications of thin cirrus clouds in the stratosphere at mid-latitudes, Atmos. Chem. Phys., 5, 3407–3414, doi:10.5194/acp-5-3407-2005, 2005.

Keckhut, P., Borchi, F., Bekki, S., Hauchecorne, A., and SiLaouina, M.: Cirrus classification at mid-latitude from systematic lidar observations, J. Appl. Meteorol. Clim., 45, 249–258, 2006.

AMTD
5, 5787–5822, 2012

Keckhut, P., Perrin, J.-M., Thuillier, G., Hoareau, C., Porteneuve, J.-P., and Montoux, N.: Subgrid-scale cirrus observed by lidar at mid-latitude: variability of the cloud optical depth, J. Appl. Remote Sens., submitted, 2012.

Khvorostyanov, V. I. and Sassen, K.: Microphysical processes in cirrus and their impact on radiation: a mesoscale modeling perspective, in: Cirrus, edited by: Lynch, D. K., Sassen, K., Starr, D. O'C., and Stephens, G., Oxford University Press, 397–432, 2002.

Lanzante, J. R.: Resistant, robust and non-parametric techniques for the analysis of climate data: theory and examples, including applications to historical radiosonde station data, Int. J. Climatol., 16, 1197–1226, 1996.

Lehmann, R., von der Gathen, P., Rex, M., and Streibel, M.: Statistical analysis of the precision of the Match method, Atmos. Chem. Phys., 5, 2713–2727, doi:10.5194/acp-5-2713-2005, 2005.

Luo, Z. and Rossow, W. B.: Characterizing tropical cirrus life cycle, evolution, and interaction with upper-tropospheric water vapor using Lagrangian trajectory analysis of satellite observations, J. Climate, 17, 4541–4563, 2004.

Montoux, N., Keckhut, P., Hauchecorne, A., Jumelet, J., Brogniez, H., and David, C.: Isentropic modeling of a cirrus cloud event observed in the midlatitude upper troposphere and lower stratosphere, J. Geophys. Res., 115, D02202, doi:10.1029/2009JD011981, 2010.

Platt, C. M. R. and Dilley, A. C.: Determination of the cirrus particle single-scattering phase function from lidar and solar radiometric data, Appl. Optics, 23, 380–386, 1984.

Rex, M., von der Gathen, P., Harris, N. R. P., Lucic, D., Knudsen, B. M., Braathen, G. O., Reid, S. J., De Backer, H., Claude, H., Fabian, R., Fast, H., Gil, M., Kyrö, E., Mikkelsen, I. S., Rummukainen, M., Smit, H. G., Stähelin, J., Varotsos, C., and Zaitcev, I.: In situ measurements of stratospheric ozone depletion rates in the Arctic winter 1991/1992: a Lagrangian approach, J. Geophys. Res., 103, 5843–5853, 1998.

Rex, M., von der Gathen, P., Braathen, G. O., Harris, N. R. P., Reimer, E., Beck, A., Alfier, R., Krüger-Carstensen, R., Chipperfield, M., De Backer, H., Balis, D., O'Connor, F., Dier, H., Dorokhov, V., Fast, H., Gamma, A., Gil, M., Kyrö, E., Litynska, I., Mikkelsen, I. S., Molineux, M., Murphy, G., Reid, S. J., Rummukainen, M., and Zerefos, C.: Chemical ozone loss in the Arctic winter 1994/95 as determined by the Match technique, J. Atmos. Chem., 32, 35–59, 1999.

AMTD
5, 5787–5822, 2012

Sanderson, B. M., Piani, C., and Ingram, W. J.: Towards constraining climate sensitivity by linear analysis of feedback patterns in thousands of perturbed-physics GCM simulations, Clim. Dynam., 30, 175–190, doi:10.1007/s00382-007-0280-7, 2008.

Sassen, K. and Campbell, J. R.: A midlatitude cirrus cloud climatology from the facility for atmospheric remote sensing. Part 1: Macrophysical and synoptic properties, J. Atmos. Sci., 58, 481–496, 2001.

Sassen, K., Wang, Z., and Liu, D.: Global distribution of cirrus clouds from CloudSat/Cloud-Aerosol Lidar and Infrared Pathfinder Satellite Observations (CALIPSO) measurements, J. Geophys. Res., 113, D00A12, doi:10.129/2008JD009972, 2008.

Sassen, K., Wang, Z., and Liu, D.: Cirrus clouds and deep convection in the tropics: insights from CALIPSO and CloudSat, J. Geophys. Res., 114, D00H06, doi:10.1029/2009JD011916, 2009.

Sherlock, V. J., Garnier, A., Hauchecorne, A., and Keckhut, P.: Implementation and validation of a Raman backscatter lidar measurement of mid and upper tropospheric water vapour, Appl. Optics, 38, 5838–5850, 1999.

Spichtinger, P. and Gierens, K. M.: Modelling of cirrus clouds – Part 1b: Structuring cirrus clouds by dynamics, Atmos. Chem. Phys., 9, 707–719, doi:10.5194/acp-9-707-2009, 2009.

Stubenrauch, C., Rossow, W., Scott, N., and Chedin, A.: Clouds as seen by satellite sounders (3I) and imagers (ISCCP). Part III: Spatial heterogeneity and radiative effects, J. Climate, 12, 3419–3442, 1999.

Taylor, J. R., Randel, W. J., and Jensen, E. J.: Cirrus cloud–temperature interactions in the tropical tropopause layer: a case study, Atmos. Chem. Phys., 11, 10085–10095, doi:10.5194/acp-11-10085-2011, 2011.

von der Gathen, P., Rex, M., Harris, N. R. P., Lucic, D., Knudsen, B. M., Braathen, G. O., De Backer, H., Fabian, R., Fast, H., Gil, M., Kyrö, E., Mikkelsen, I. S., Rummukainen, M., Stähelin, J., and Varotsos, C.: Observational evidence for chemical ozone depletion over the Arctic in winter 1991–92, Nature, 375, 131–134, 1995.

AMTD
5, 5787–5822, 2012

Table 1. Transmitter and receiver characteristics of the OHP and RTV lidar systems.

	Rome-RTV (41.8° N, 12.6° E, 107 m a.s.l)			OHP (43.9° N, 5.7° E, 678 m a.s.l)		
Transmitter						
Laser Type	Nd : Yag			Nd : Yag		
Wavelenght	532 nm–355 nm			532 nm		
Energy per pulse	200 mJ–400 mJ			400 mJ		
Pulse repetition rate	10 Hz			50 Hz		
beam diameter	45 mm			20 mm		
beam divergence	0.1 mrad			0.4 mrad		
	Collector 1	Collector 2	Collector 3	Collector 1	Collector 2	Collector 3
Receiver						
Type of telescope	Newtonian array	Newtonian	Newtonian	Newtonian array	Newtonian	Newtonian
Diameter, *f*-number	9 × 500 mm, F3	300 mm, F3	150 mm, F3	4 × 500 mm, F3	800 mm, F3	100 mm, F2
Field of view (mrad)	0.6	0.9	1.8	0.4	0.7	10
Optic fiber	yes	yes	yes	yes	yes	yes
Data acquisition						
Raman channels N_2	387 nm	387 nm			607 nm	
H_2O	407 nm	407 nm			660 nm	
Elastic channels	532 nm	532 nm	532 nm	532 nm		532 nm
Sounding range (km)	2–15 (Raman)	0.1–5 (Raman)			2–10 (Raman)	
	25–80 (elastic)	6–40 (elastic)	0.5–8 (elastic)	25–80 (elastic)		0.2–30 (elastic)
Time resolution (sec)	60	60	60	160	160	160
Vertical resolution (m)	75	75	75	75	75	75

AMTD
5, 5787–5822, 2012

Table 2. Night-time lidar sessions, common days of measurements and Match sessions acquired during the period 2007–2008 by the OHP and RTV lidar systems.

2007–2008	OHP	RTV	common days	Match sessions
# Lidar sessions	306	71	42	4

AMTD
5, 5787–5822, 2012

Table 3a. Characterization of cirrus quasi-stationary periods identified at OHP through principal lidar parameters. Temperature values are derived from the operational radiosoundings launched from Nimes (80 km west from OHP).

UTC	18:48–19:20	21:38–22:50	22:53–23:41	23:43–01:46
Occurrence (min)	32	72	48	123
Geometric mean height (km)	11.42	11.15	11.40	11.30
Thickness (km)	0.5	1.0	1.0	0.8
Intensity of the mean BSR	7.6 ± 3.8	1.3 ± 0.2	9.0 ± 8.8	2.4 ± 1.2
Relative height (km)	0.19	−0.05	0.16	0.06
Mean T inside the cloud (K)	211	212	211	211
Optical depth (PI method, LR = 18.2 sr)	0.026 ± 0.001	0.051 ± 0.001	0.024 ± 0.001	0.009 ± 0.001
Optical depth (MI method)	0.021 ± 0.005	0.011 ± 0.007	0.008 ± 0.009	0.011 ± 0.011

AMTD
5, 5787–5822, 2012

Table 3b. Characterization of cirrus quasi-stationary periods identified at RTV through principal lidar parameters. Temperature values are derived from the operational radiosoundings launched from Pratica di Mare (25 km south-west from RTV).

UTC	19:31–20:43	20:44–21:51	21:52–23:06	23:07–23:36	23:37–00:50
Occurrence (min)	72	67	74	29	73
Geometric mean height (km)	10.75	10.90	11.10	11.10	11.20
Thickness (km)	1.07	1.3	0.7	0.6	0.7
Intensity of the mean BSR	1.4 ± 0.4	1.6 ± 0.7	1.9 ± 0.7	2.5 ± 1.6	2.4 ± 1.6
Relative height (km)	−0.35	−0.20	0.00	0.00	0.05
Mean T inside the cloud (K)	216	215	214	214	214
Optical depth (PI method, LR = 18.2 sr)	0.003 ± 0.001	0.007 ± 0.001	0.005 ± 0.001	0.008 ± 0.001	0.011 ± 0.001
Optical depth (MI method)	0.011 ± 0.008	0.005 ± 0.027	0.031 ± 0.033	0.018 ± 0.091	0.027 ± 0.081
Optical depth (Raman method)	0.011 ± 0.008	0.007 ± 0.007	0.004 ± 0.03	–	0.029 ± 0.053

AMTD
5, 5787–5822, 2012

Table 4. Estimates of effective ice crystal radius (r) derived from Eq. (1) for the values of Δz and τ of the cirrus quasy-stationary periods considered in the Match approach. Calculations are made for five different ice crystal number concentrations (N_0).

N_0 [number cm^{-3}]	OHP r [µm]	RTV r [µm]
0.05	12.9	6.0
0.1	9.1	4.3
0.5	4.1	1.9
1	2.9	1.3
5	1.3	0.6

AMTD
5, 5787–5822, 2012

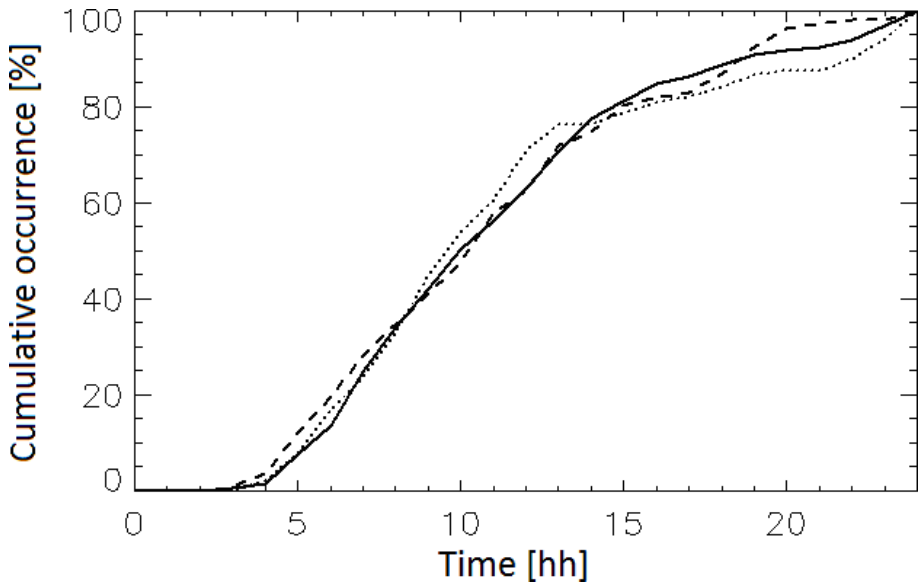

Fig. 1. Cumulative occurrence (in %) of the OHP-RTV air mass coincidence in function of the time spent by the air masses (at 8, 10 and 12 km, solid, dashed and dotted lines, respectively) to go from OHP to RTV sites. Backward trajectories have been computed for 5-yr period (2006–2010).

AMTD
5, 5787–5822, 2012

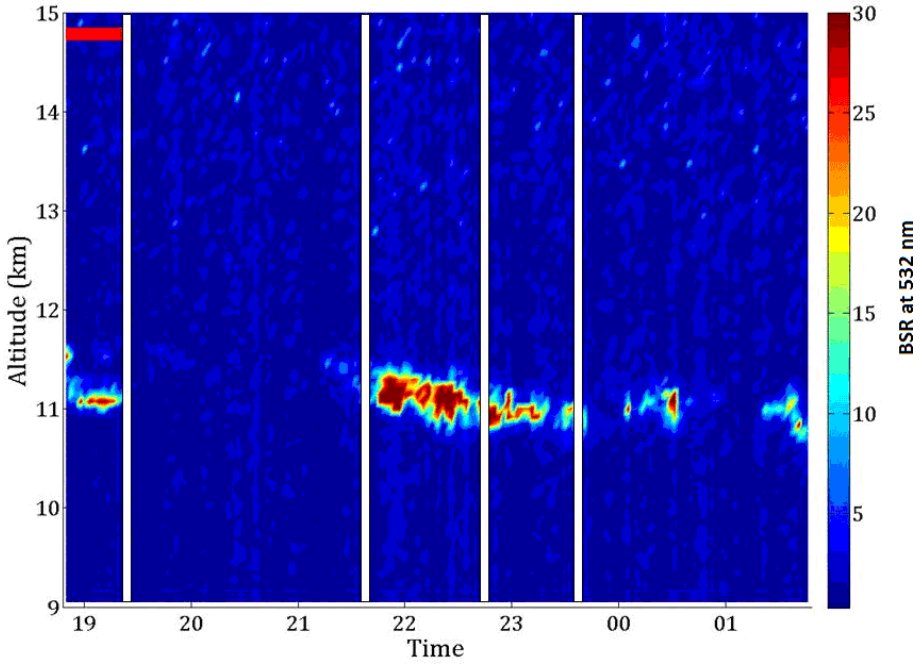

Fig. 2a. Contour plot of the backscattering ratio (BSR) calculated from the elastic channel at 532 nm for the lidar session at OHP between 18:48 and 01:44 UTC. White vertical lines identify the quasi-stationary periods. The horizontal red bar indicates the quasi-stationary period used in the Match approach (18:48–19:20 UTC).

AMTD
5, 5787–5822, 2012

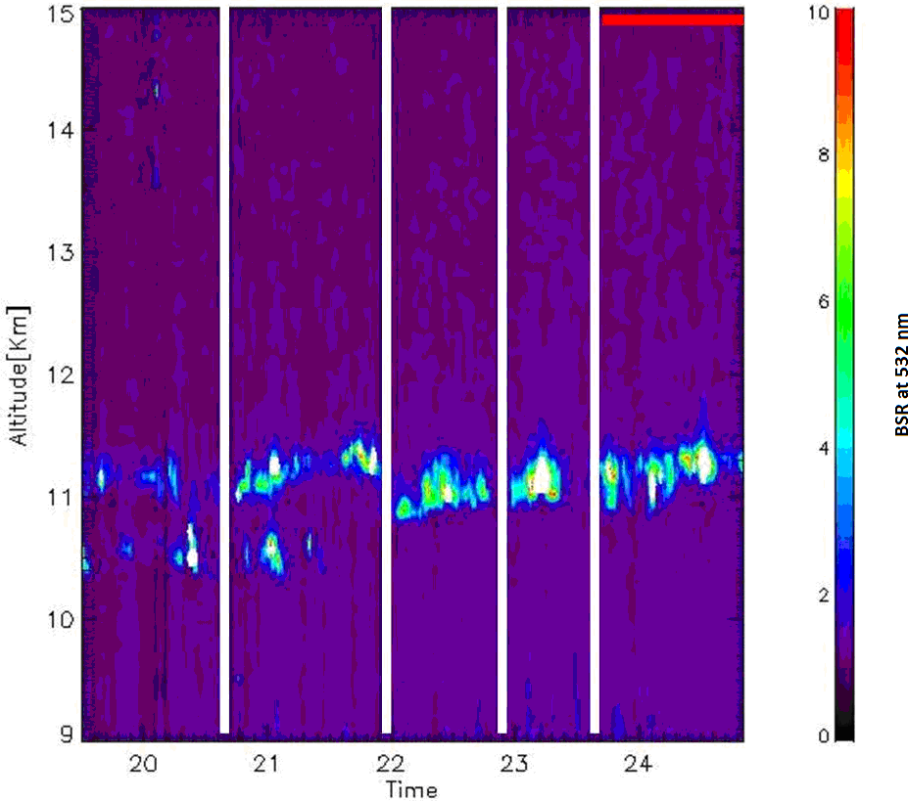

Fig. 2b. Contour plot of the backscattering ratio (BSR) calculated from the elastic channel at 532 nm for the lidar session at RTV between 19:31 and 00:50 UTC. White vertical lines identify the quasi-stationary periods. The horizontal red bar indicates the quasi-stationary period used in the Match approach (23:37–00:50 UTC).

AMTD
5, 5787–5822, 2012

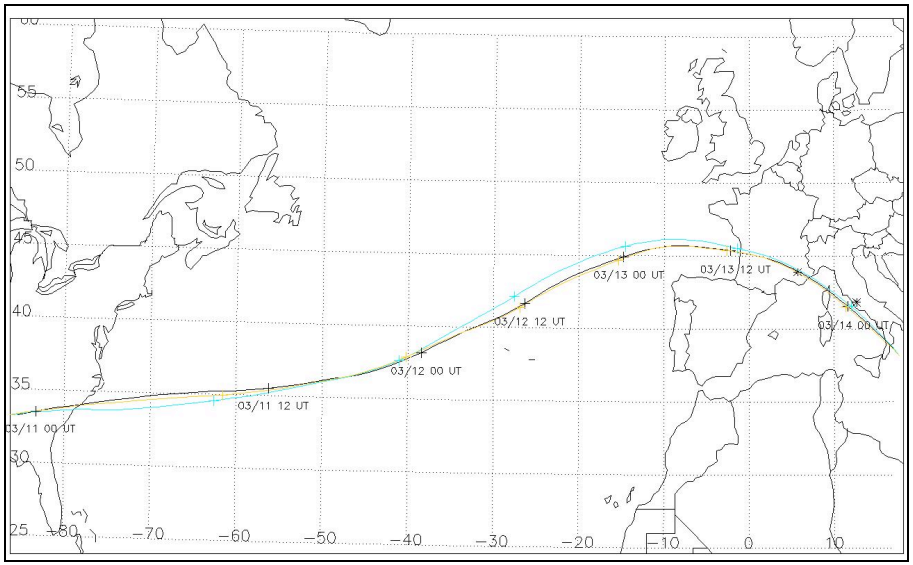

Fig. 3. Backward trajectories initialized 14 March 2008 at 01:00 UTC until 11 March 2008 at 01:00 UTC for three atmospheric levels (10.7, 11.2, 11.7 km, black, yellow and blue, respectively) that include bottom and top heights of the cirrus observed by OHP and RTV lidars. Stars points denote the positions of OHP (43.9° N/5.7° E) and RTV (41.8° N/12.7° E) sites, while plus points indicate the air mass temporal position every 12 h.

AMTD
5, 5787–5822, 2012

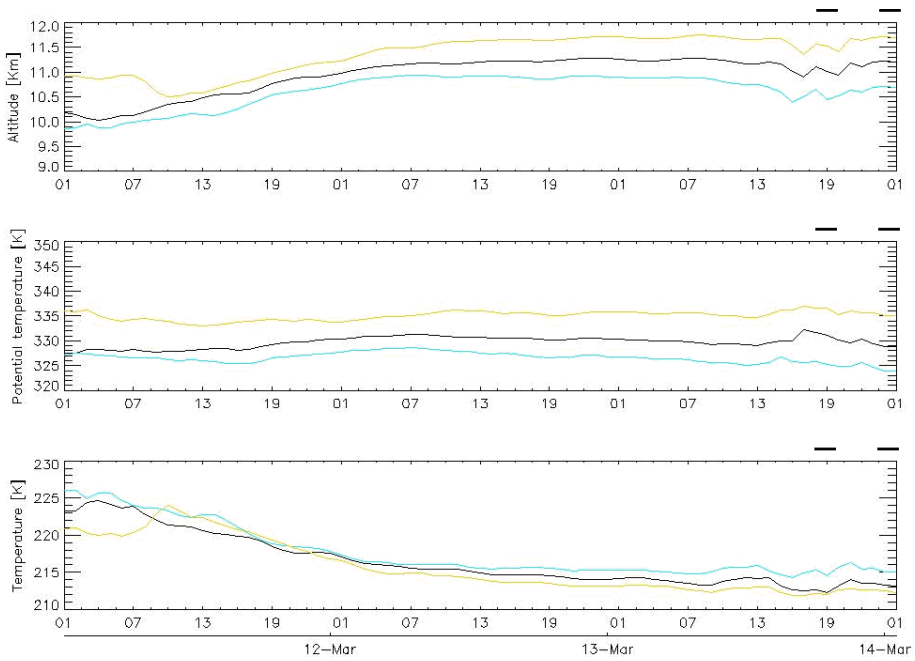

Fig. 4. Evolution of the altitude, potential temperature and temperature of the air mass backward trajectories between 11 March 2008 at 01:00 UTC and 14 March 2008 at 01:00 UTC for three atmospheric levels (10.7, 11.2, 11.7 km, black, yellow and blue, respectively) that include bottom and top heights for the cirrus observed by OHP and RTV lidars. Horizontal delimited black bars indicate air mass passage above OHP and RTV sites (13 March 2008 at around 19:00 UTC and 14 March 2008 at 01:00 UTC, respectively).

AMTD
5, 5787–5822, 2012

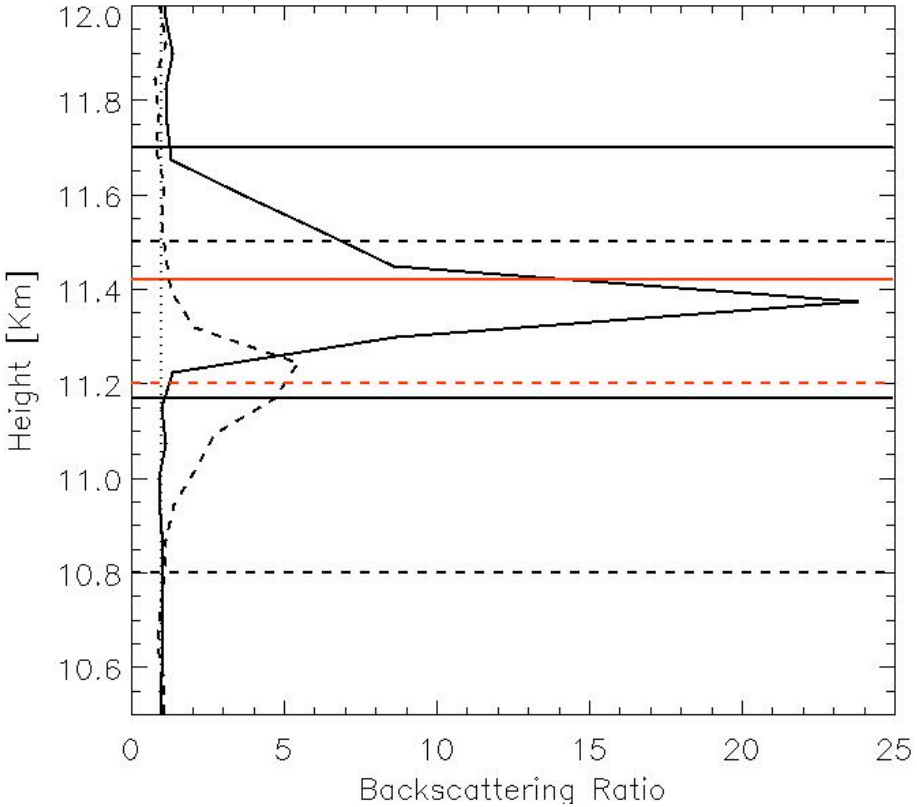

Fig. 5. Backscattering ratio profiles of the cirrus measured at OHP for the first quasi-stationary period (18:48–19:20 UTC, continuous line) and at RTV for the last quasi-stationary period (23:37–00:50, dashed line). Horizontal black lines identify the cirrus top and base heights, while the red lines indicate cirrus mid-heights.

AMTD
5, 5787–5822, 2012